Nuclear Engineering and Design 373 (2021) 111032

Contents lists available at ScienceDirect

Nuclear Engineering and Design

journal homepage: www.elsevier.com/locate/nucengdes

Nusselt correlation development in unsteady laminar gas flows for CABRI multiphysic simulations with CATHARE2

J-M. Labit [a], N. Seiler [a,*], O. Clamens [a], E. Merle [b]

[a] CEA, DES, IRESNE, Cadarache, F-13108 Saint Paul-Lez-Durance, France
[b] CNRS-IN2P3-LPSC/Grenoble INP/UGA, 53 Rue des Martyrs, 38026 Grenoble Cedex, France

ARTICLE INFO

Keywords:
CABRI
Multiphysics
RIA
Nusselt
Transient laminar compressible gas flow
CATHARE

ABSTRACT

CABRI is an experimental pulse reactor, which aims at studying and thus at better understanding RIA (Reactivity Initiated Accident) effects on nuclear fuels. The restart of the CABRI reactor in 2015 offers the opportunity to validate tools involving multiphysic calculation schemes on reactivity insertions (RI) transients at a system scale. The reactivity insertion in CABRI is mastered by the depressurization of a neutron absorber (^{3}He), contained into transient rods. This enables the realization of various types of transients. As this depressurization highly influences the reactivity insertion kinetics, it is essential to accurately simulate the ^{3}He density evolution which depends on the heat exchanges inside the circuit. The challenge is thus to manage the simulation of the various CABRI complex transients. Previous work allowed to model with CATHARE2 the whole reactor with its specific phenomena as well as phenomena generally involved in RIA, for instance strong neutronic feedback effects, effect of the pellet-clad interaction on the gap conductance and transient heat exchanges between fuel rods and water. These studies also revealed that some CABRI transients were still difficult to model with CATHARE2 and this paper shows the necessity to catch the transient heat exchanges in the transients rods for the simulation of the power pulse in CABRI reactor. In order to achieve this objective, a correlation for the Nusselt evolution in an unsteady compressible laminar ^{3}He flow, inside a closed tube, has been realized from numerical resolution of an analytical model and implemented in the scientific calculation tool CATHARE2. This paper describes this analytical model and its numerical resolution. After having been validated on results of the literature in steady flow inside open tube, the correlation established for the evolution of the Nusselt in a transient rods' tube is given. Finally, Best-Estimate simulation results of CATHARE2 are compared with experimental data obtained on CABRI commission tests: core power and ^{3}He pressure evolution.

1. Introduction

This work is part of a broader effort leading to the improvement and validation of the multi-physics modeling of CABRI-RIA transients with the system simulation tool CATHARE2 (Labit et al., 2020a, 2020b). The CABRI reactor is an experimental pulse pool-type research reactor, funded by IRSN and operated by CEA at the Cadarache nuclear center in France (Hudelot et al., 2016). It is designed to experimentally simulate a sudden and quasi-instantaneous power excursion, known as a power transient, typical of a Reactivity-Initiated Accident. This type of accident is considered in the safety analysis of various types of reactors. The CABRI experiments constitute a real opportunity to collect valuable data on such complex multiphysic transients. In the CABRI core, the ^{3}He depressurization from the transient rods injects up to 4$ of reactivity triggering the power excursion. Thus, power pulses can reach a maximal instantaneous power around 20 GW with a Full Width at Half-Maximum (FWHM) around 10 ms. This reactor provides various kinds of power pulses by controlling the ^{3}He depressurization (FWHM between 9–90 ms and power peak between 1 and 21 GW).

Previous works (Labit et al., 2020a, 2020b) have led to the development of a dedicated version of CATHARE2 which handles and reproduces transient coupled multiphysic phenomena in CABRI reactor. CATHARE2 (Geffraye et al., 2011; Emonot, 2011) has been developed by four French partners: CEA, IRSN, EDF and FRAMATOME. This highly verified and validated tool is intended, among other things, for safety analyses with best estimate calculations of thermal–hydraulics transients in PWRs for postulated accidents or other incidents and quantification of conservative margins. The description of thermal non-equilibrium inhomogeneous two-phase flow is based on a two-fluid

* Corresponding author.
E-mail address: nathalie.marie@cea.fr (N. Seiler).

https://doi.org/10.1016/j.nucengdes.2020.111032
Received 25 September 2020; Received in revised form 14 December 2020; Accepted 15 December 2020
Available online 28 January 2021

Nomenclature

Acronyms

BC	Boundary condition
CABRI	French experimental reactor dedicated to safety studies
CATHARE	Code for Analysis of THermalhydraulics during an Accident of Reactor and safety Evaluation
CEA	Commissariat á l'Energie Atomique et aux Energies Alternatives (French Alternative Energies and Atomic Energy Commission)
CSR	Control and Safety Rods
DD	Double depressurization via the low flowrate first, and second the high flowrate channel
EDF	Electricité De France
FWHM	Full Width at Half-Maximum
IRSN	Institut de Radioprotection et de Sûreté nucléaire (Institute for Radiological protection and Nuclear Safety)
PWR	Pressurized Water Reactor
RIA	Reactivity Initiated Accident
SD1, SD2	Single depressurization via the high flowrate and low flowrate channel respectively
TOP	Transient OverPower
VABT03, VABT04	Control valves, respectively of the high flowrate and low flowrate channel

Mathematical operators and variables

Δ	Laplacian
div	Divergence
$\overrightarrow{\text{grad}}$	Gradient

Physical variables

α	Thermal diffusion coefficient of water ($m^2 \cdot s^{-1}$)
β_{eff}	Effective delayed neutrons fraction (pcm)
η	Dynamic viscosity (Pa·s)
c_p	Heat capacity ($J \cdot kg^{-1} \cdot K^{-1}$)
λ	Conductivity ($W \cdot m^{-1} \cdot K^{-1}$)
ϕ	Heat flux ($W \cdot m^{-2}$)
$\rho^\star$	Normalized density
ρ	Density ($kg \cdot m^{-3}$)
τ	Characteristic time (s) taken equal to depressurisation duration
Θ	Nondimensionnalized temperature
γ	Heat capacity ratio
C_v	Valve capacity
D_h	Hydraulic diameter (m)
Fo	Fourier number
h	Heat exchange coefficient ($W \cdot m^{-2} \cdot K^{-1}$)
h_{04}	Valve stem position (mm)
L	Tube length (m)
Nu	Nusselt number
P	Pressure (Pa)
P_0	Initial pressure (Pa)
Pr	Prandtl number
R	Ideal gas constant (J/mol/K)
R	Tube radius (m)
r	Radial coordinate (m)
$r^\star$	Normalized radial position
r_x	Gas constant specific to gas x (J/kg/K)
Re	Reynolds number
T	Temperature (K)
$t^\star$	Normalized time
v	Fluid velocity (m/s)
V_r	Normalized radial velocity
v_r	Radial velocity (m/s)
V_z	Normalized axial velocity
v_z	Axial velocity (m/s)
x_T	Maximal pressure drop ratio in the valve
Y	Expansion factor in the valve
z, x	Axial coordinate (m)
$z^\star$	Normalized axial position

Subscripts

0	Initial (or reference for nondimensionnalization)
w	Wall

approach and six-equation model, using mainly algebraic constitutive relations for the modelling of interfacial coupling, wall friction, and wall heat transfer processes. This dedicated version of CATHARE2 (Labit et al., 2020b) gathers main improvements in order to accurately simulate main influential phenomena occurring during such reactivity insertion transients (established from a QPIRT Labit et al., 2019);

- notably the improvement of the neutronic point-kinetics method to handle 3D effects inside the core and the improvement of feedback effects computation (like Doppler and clad expansion feedback effects);
- the thermal–hydraulic wall to fluid heat transfers in very fast transient conditions and associated flow configurations;
- the thermal-mechanic effect of the pellet-clad interaction on the gap conductance.

The modelling of CABRI transients is performed with CATHARE2 and takes into account, in addition to previous phenomena:

- the ^{3}He depressurization through the modeling of the whole transient rods circuit and its regulating valves with sonic flows occurrence;
- the coupling between the core reactor circuit and the transient rods circuit: evolution of the external reactivity insertion according to the ^{3}He density evolution. Moreover, the multiphysic 'TOP' effect is modeled. This effect is due to helium ionization inside the core that, makes the ^{3}He temperature increase and its density decrease. This finally impacts the global core neutronics. This reaction adds a power density inside the transient rods.

Results of CATHARE2 have been compared to experimental results for nine CABRI commission tests determined according to a validation methodology presented in Labit et al. (2020b) and presented good consistency. However, it arises from preliminary sensitivity evaluations that the simulations of transients with slow ^{3}He depressurization present large discrepancy with the experimental power transient shape and particularly on the peak instant, in spite of the good agreement observed on the ^{3}He pressure evolution (Labit et al., 2020b). First analyses show that, even if the evolution of the ^{3}He pressure in these tests is well simulated, the reactivity insertion is too low. This leads to presume that the simulated ^{3}He density is too high, and thus its temperature is lower than in the experiment. The heat transfer coefficient in CATHARE2 between the ^{3}He flow and the wall of the transients rods is thus questionable. Indeed, this coefficient is given by a Nusselt number obtained in a open heated tube in steady-state for a non-compressible flow, whereas ^{3}He flow in transient rods is unsteady and compressible in a closed heated tube.

Nowadays, most correlations used for both single and two-phase

flows in system or component thermal–hydraulics simulation tools are still issued from steady-state experiments: Dittus-Boelter, Colburn, Sieder-Tate, Thom, Rosenhow *etc*. This is the case in CATHARE2 (Geffraye et al., 2011), RELAP5 (RELAP5/MOD3.2, 1995), ATHLET (Austregesilo et al., 2003) and TRACE (Staudenmeier, 2004). Some studies have been conducted in this field in order to better understand the heat exchange phenomena during fast transients in both single and two-phase flows. Some developments have been made and implemented in CATHARE2 in that purpose (Labit et al., 2020a) concerning the heat exchanges inside the core. But the heat exchanges seem to be unsufficiently modelled with common-used correlations inside the transient rods too. This paper raises thus the issue of gas single-phase transient heat exchanges during depressurizations.

2. Context

2.1. The CABRI core and its transient rods

CABRI is a water-cooled reactor able to reach 23.7 MW power level for steady state (Hudelot et al., 2016). Its core consists of 1487 UO_2 fuel rods (enrichment: 6%), reaching the initial conditions by means of 6 Control and Safety Rods in hafnium (cf. Fig. 2). One of the main particularities of the reactor is its reactivity injection system which is used to initiate and shape the power transients. The RIA transients considered in safety demonstration postulate, for PWR, the ejection of a control rod as accident initiator. The very rapid increase in reactivity due to a potential control rod ejection is recreated inside the CABRI reactor by the depressurization of ^{3}He from four "transient rods" located inside the core and connected to low and high flow rate channels towards a dump tank. These transient rods enable the realization of various types of transients. Depressurizations that are made through high flow rate channel are called "SD1" (Simple Depressurization way 1), and the ones that are made through low flow rate channel are called "SD2". In order to be representative of accidental power plant conditions and manage the shape of the power pulse, the depressurization can be done by opening successively the fast opening valves of the low flow rate and then the high flow rate channels (called "Double Depressurizations" DD). The transient rods circuit is detailed in Fig. 1,2. We can see the high flowrate channel (for SD1) consisting of the successive fast valve VABT01 and control valve VABT03 and the low flowrate channel (for SD2) with its valves (VABT02 and VABT04). Each transient rod is composed of 24 tubes of an internal diameter equal to 8.8 mm, plunged into the core.

Before the test, the transient rods are filled with ^{3}He and the core power is stabilised around 100 kW. The power transient is initiated by opening the fast valves so that the helium under pressure can escape. This results in a sudden increase of reactivity (since the neutrons are no more absorbed by the ^{3}He, the fission rate increases) and thus of power (the pulse). This is immediately limited by neutron counter-reactions, mainly Doppler feedback effect, then at a lower level, clad expansion and moderating feedback effects. When the difference between initial insertion of reactivity (induced by ^{3}He depressurization) and anti-reactivity becomes lower than 1$, the core power decreases. Finally, the core is completely shut down by the control rods drop. The pulses last from several milliseconds to several tens of milliseconds, with instantaneous power up to 21 GW, and the energy deposited in the core can then reach up to 250 MJ before the control rods drop. The core is cooled with a forced convection water loop and the whole system is immersed in a pool.

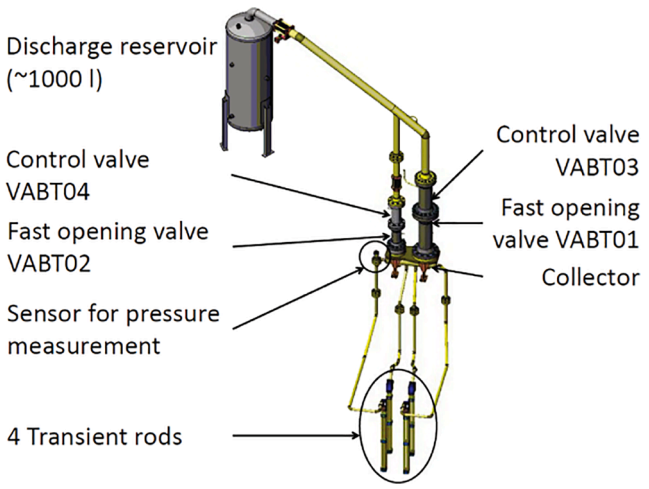

Fig. 1. Transient rods circuit.

An example of such a transient results is given in Fig. 2 by their ^{3}He pressure and power evolutions. The initial ^{3}He pressure and its kinetics of depressurization in the four transient rods circuit can lead to many kinds of power pulses, with various heights and widths at half-maximum. Transients are thus characterized by their maximum power, by their Full Width at Half Maximum (FWHM) and by the energy deposit into the core. Thus the short FWHM power transients will be generated by the opening of the unique high flow rate channel. The maximum power is then very high (10 to 20 GW) and the FWHM is short (~10 ms), due to the reactivity insertion dynamics. The energy deposit in this case depends on the initial pressure in the transient rods, the control valve aperture and the control rods drop time.

2.2. Simulation of CABRI transients with CATHARE2

The simulation of CABRI transients with CATHARE2, widely described in Labit et al. (2020b), consists in a modelling of both circuits of CABRI and a dynamic coupling of the transient rods with the core and the cooling system. The depressurization is accurately modelled with CATHARE2 and the density evolution, at each time step, allows to compute the external reactivity inside the core and then, with a point kinetic method, the core power. CATHARE (Code for Analysis of THermalhydraulics during an Accident of Reactor and safety Evaluation) is a two-phase thermal–hydraulic simulation tool in development since 1979 in France. The software is currently in its second major revision (CATHARE2) and is used, in particular, in pressurized water reactor safety analyses. The CATHARE2 tool has a modular structure capable of operating in 0D, 1D or 3D. It is able to model any type of reactor with several types of system loop. The software is based on a thermal–hydraulic two-phase model with six equations (conservation of mass, energy and momentum for each phase). This tool involves also a point-kinetic neutronic model and a thermomechanical model for the solid deformations computation. The successive versions of the code were verified and validated in a two-step process: validation in separate-effect experiments followed by validation of the overall behaviour of the tool in integral experiments. Given its capabilities and its validation domain, this calculation tool has become in France the main thermal–hydraulic code for safety demonstration, and is widely used by the CEA, IRSN, EDF, Framatome etc.

After having reviewed the current capabilities of the CATHARE2 tool, some improvements have been performed in order to be representative of phenomena that are specific on one hand to RIA, and on the other hand to CABRI. The dedicated version of CATHARE2 for RIA and the modelling of CABRI have been demonstrated to very well perform the simulation of SD1. The average difference computation/experiment is less than 6% on maximal power, 2% on energy deposit and −5% on FWHM (Labit et al., 2020b).

2.3. Need of improvement

Research led in the modelling of CABRI transients revealed that even if SD1 were very well simulated with CATHARE2, results for SD2 and DD

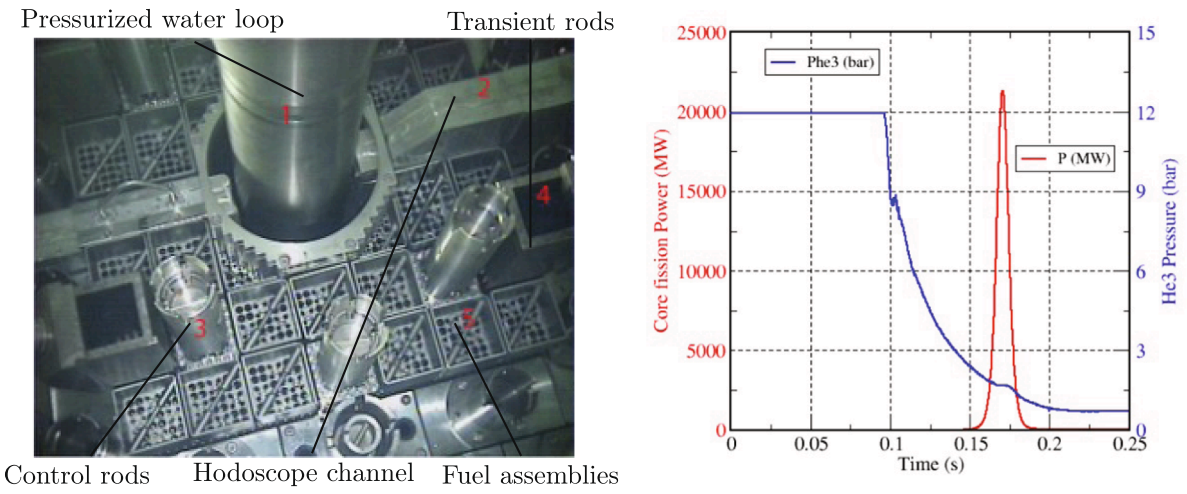

Fig. 2. A view of the CABRI core and an example of power pulse and depressurization of transients rods.

could be significantly improved, as observed in Labit et al. (2020b). The simulations of SD2 and DD transients give a power pulse that is slightly delayed in comparison with the experiments. This leads to a power pulse higher than the experimental one. As a consequence, the effect of the delay in the simulated reactivity insertion is especially much more significant during a DD. Indeed, in this kind of transient, the high flowrate channel is opened before the end of the depressurization, what sharply changes the reactivity insertion. Fig. 3 illustrates this phenomenon: dashed lines represent helium pressure evolution and plain ones power evolution. If the prompt-criticality is not reached before the opening of the second channel, reactivity is mostly injected later during the depressurization via the high flowrate channel ("SD1" part), leading to a largely overestimated power pulse, corresponding to the one that could be obtained with a SD1. This power pulse is then very high and narrow.

According to further investigations and sensitivity studies from Clamens (2018), the peak instant issue can be due to two lacks in the modelling:

- the core kinetics modelling, based on a point kinetics, does not allow to make the kinetics parameters, neutron flux distribution and spectrum vary with time (Larmash, 1966; Labit et al., 2020b). This variation could be more significant during SD2 than during SD1;
- the depressurization speed.

We noticed a lack in CATHARE on laminar heat exchanges that can impact significantly the depressurization speed. Indeed, if the heat exchanges are underestimated, the helium temperature inside the rods is too low. The helium density inside the rods is then too high and its absorption macroscopic cross section is still too high. The reactivity insertion is then delayed. The reason why this phenomenon is not significant during SD1 is that these depressurizations are very quick: less than 0.2 s. SD2 and, then, DD are longer (around 2 s), sufficiently for heat exchanges inside the rods to have an influence.

In addition to that, gas flow in the transient rods can reach very low velocities during SD2. By studying more precisely these depressurizations (SD2) with CATHARE2, we can observe that the flow is laminar inside the rods.

2.4. Literature review on laminar Nusselt number

CATHARE2 uses common values for steady-state Nusselt number in laminar developed flows (Incropera and Dewitt, 1996; Shah and London, 1978):

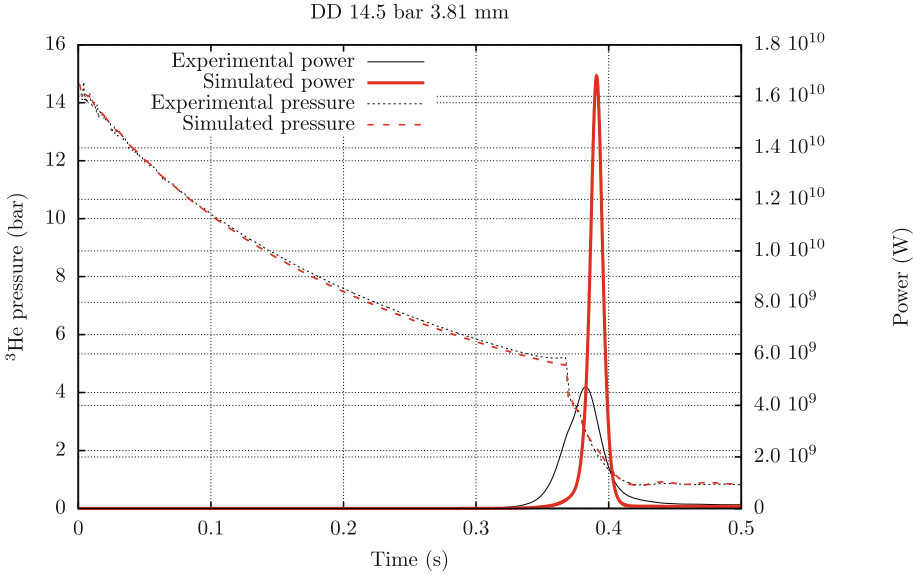

Fig. 3. First simulation of a double-depressurization with CATHARE2.

- with constant heat flux at the wall, the Nusselt number is equal to 4.36;
- with constant wall temperature, the Nusselt number is equal to 3.66.

For gas flowing into a metallic tube, the ratio of gas effusivity over metal effusivity is very low, so that the wall temperature can be considered as constant. So, for a laminar flow of gas in CATHARE2, it has been considered that $Nu = 3.66$. This value is derived from an analytical resolution, performed by E.W. Nusselt in 1910 (Nusselt, 1910; Belhocine and Wan Omar, September 2018). The situation of the study is an gas flow inside open tube (radius R), heated to a constant temperature. The assumptions are:

- the flow is laminar;
- the velocity profile is established;
- the flow is incompressible and steady.

From these assumptions, we deduce that the profile is a Poiseuille profile. The energy conservation equation is so written as:

$$\rho c_p \left(\overrightarrow{v}\cdot\overrightarrow{\text{grad}}\right)T + \text{div}\left(-\lambda\overrightarrow{\text{grad}T}\right) = 0 \tag{1}$$

If we assume properties of the fluid as constant, and axial conduction as negligible, we obtain:

$$2v_0\left(1-\left(\frac{r}{R}\right)^2\right)\frac{\partial T}{\partial z} - \alpha\frac{1}{r}\frac{\partial}{\partial r}\left(r\frac{\partial T}{\partial r}\right) = 0 \tag{2}$$

Where v_0 is the cross-section averaged velocity in the pipe. This equation can be solved by a very complex way (Belhocine and Wan Omar, September 2018; Nusselt, 1910). Considering that $\phi = h(T_w - \overline{T}) = -\lambda\partial T/\partial r|_0$ (where $\overline{T}$ is the fluid cross-section averaged temperature), E.W. Nusselt deduced what has been called now in the literature the "Nusselt number":

$$Nu = \frac{hD_h}{\lambda} = \frac{-D_h\frac{\partial T}{\partial r}\Big|_0}{T_w - \overline{T}} \tag{3}$$

From the analytical temperature profile, E.W. Nusselt deduced the value of this number. It tends towards 3.656, whatever the fluid properties, the average velocity, the geometry or the boundary conditions. In this case of thermally developing flow, the evolution of Nusselt number as a function of the position x in the tube is very well approached by the Shah-London correlation (Shah and London, 1978):

$$Nu = \begin{cases} 1.077(x^\star)^{-1/3} - 0.7 & \text{if} \quad x^\star \leqslant 0.001 \\ 3.657 + 6.874(1000x^\star)^{-0.488}\text{e}^{-57.2x^\star} & \text{if} \quad x^\star > 0.001 \end{cases} \tag{4}$$

where:

$$x^\star = \frac{1}{RePr}\frac{x}{D_h} \tag{5}$$

Unfortunately, this correlation is not representative of the gas flow inside the transient rods. Indeed:

- the gas flow in the rods is not incompressible, nor is it steady and its properties are, at first glance, variable with r, regarding the quite high temperature gradients that can occur during SD2 (the gas can reach temperatures of −30 °C and the wall is at a temperature of 20 °C);
- the geometry is very different from the geometry of the transient rods, due to the fact that the tubes are closed at one side. As a consequence, the flow is clearly unsteady and the velocity profile cannot be taken equal to the velocity profile that could be observed during a steady and incompressible flow.

No more references that could help to model heat exchanges in such a specific configuration have been found, for transient and compressible laminar flow. Reference Presler (1971) deals with the heat exchanges during developping laminar gas flow, but in steady-state and for an open tube geometry. Their strategy is to solve numerically (with finite-differences method) the gas flow conservation equations in steady-state in order to obtain the Nusselt number evolution inside the tube. But this is not representative of our case.

Some preliminary studies have shown that added terms in Eq. (1) changed significantly the Nusselt number, especially the established Nusselt number when $x \to +\infty$. These terms correspond, in our situation, to unsteady terms in the energy conservation energy:

- $\partial P/\partial t$, that is very significant during the gas depressurization;
- $\partial T/\partial t$, corresponding to the temperature decrease inside the rods.

Modifying the velocity profile highly influences the temperature profile and, then, the Nusselt number too. However, taking into account variable properties in the flow did not have significant effects. This is consistent with observations made in Presler (1971).

In order to get the Nusselt number evolution during the depressurization of the transient rods, we intend to solve numerically the conservation equations of the flow inside the transient rods during the depressurization. The objective is to obtain the temperature profile and deduce the Nusselt number considering Eq. (3). This numerical model shall be able to solve 2-D unsteady flow inside the rods (the flow can be considered as being axisymmetric around the rods axis).

3. Unsteady laminar gas flow modelling

This section details the hypotheses of the study, the system considered for the modelling of the unsteady gas flow inside the rods and the boundary conditions depending on the geometry.

3.1. Assumptions

The compressible gas flow is laminar in a cylindrical tube. The problem is axissymetric around the tube axis (that is now defined as z-axis). We have:

$$\overrightarrow{v} = v_r\overrightarrow{u_r} + v_z\overrightarrow{u_z} \tag{6}$$

We assume that the gas follows the ideal gas law. This law is valid at least until pressures around 20 bar. We have drawn on Fig. 4 the difference between real gas law (van der Waals) and ideal gas law for the range of pressures encountered in CABRI transient rods. We can observe that the density difference even at 20 bar is lower than 2% between both laws. This assumption of ideal gas law behaviour is then valid.

Concerning the force balance, the effect of gravity on the gas flow is negligible as well as its work. In the energy conservation equation, axial diffusion terms (conduction and viscosity volumetric forces along z-axis) and the work of the viscosity forces are negligible too. The gas properties (conductivity, viscosity) are assumed to be constant. This choice has been made from prelimary sensitivity calculations and from literature review that have shown that the influence of their variability is very slight (Presler, 1971).

3.2. System of equations

There are 5 unknowns in that problem: radial velocity v_r, axial velocity v_z, density ρ, pressure P and temperature T. The equations of the flows are:

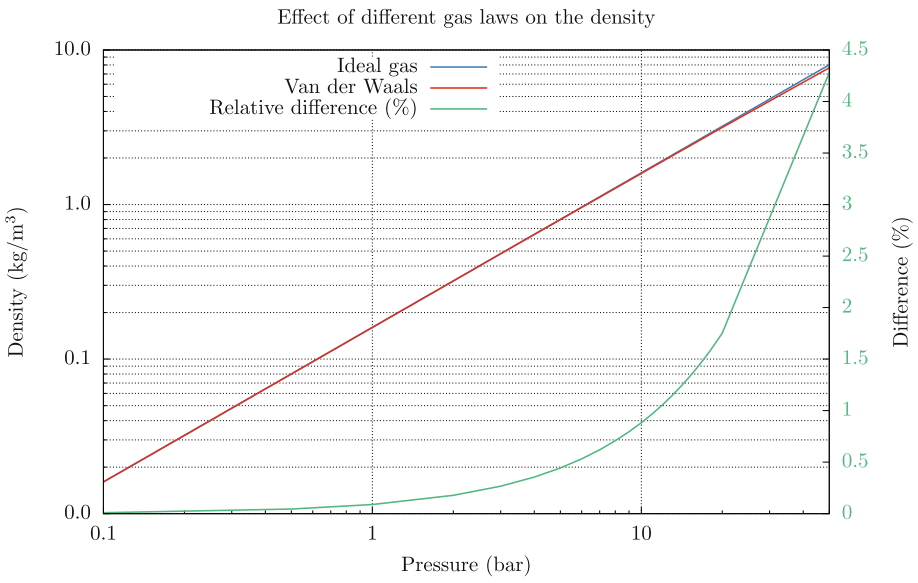

Fig. 4. Comparison of ^{3}He density with ideal and real gas laws.

$$\begin{cases} \dfrac{\partial \rho}{\partial t} + \mathrm{div}(\rho \vec{v}) = 0 & \text{(7a)} \\ \rho\left(\dfrac{\partial v_z}{\partial t} + \vec{v}\cdot\overrightarrow{\mathrm{grad}} v_z\right) = -\dfrac{\partial P}{\partial z} + \eta \Delta v_z & \text{(7b)} \\ \rho\left(\dfrac{\partial v_r}{\partial t} + \vec{v}\cdot\overrightarrow{\mathrm{grad}} v_r\right) = -\dfrac{\partial P}{\partial r} + \eta \Delta v_r & \text{(7c)} \\ \rho\left(\dfrac{\partial}{\partial t}\left(c_p T + \dfrac{1}{2}v^2\right) + \vec{v}\cdot\overrightarrow{\mathrm{grad}}\left(c_p T + \dfrac{1}{2}v^2\right)\right) = \dfrac{\partial P}{\partial t} - \mathrm{div}\left(-\lambda\overrightarrow{\mathrm{grad}} T\right) & \text{(7d)} \\ P = \rho r_{He} T & \text{(7e)} \end{cases}$$

e.g. mass conservation, momentum conservation on z and r directions, total energy conservation and equation of state of the gas. By calculating orders of magnitude of radial and axial velocities, we can show that:

$$\frac{\partial P}{\partial r} \ll \frac{\partial P}{\partial z} \tag{8}$$

We then made the usual assumption in laminar flows (Presler, 1971):

$$\frac{\partial P}{\partial r} = 0 \tag{9}$$

Thus, we can rewrite the system of equations by considering constant properties of the fluid, and neglecting axial diffusion terms:

$$\begin{cases} \dfrac{\partial \rho}{\partial t} + \dfrac{1}{r}\dfrac{\partial}{\partial r}(r\rho v_r) + \dfrac{\partial}{\partial z}(\rho v_z) = 0 & \text{(10a)} \\ \rho\left(\dfrac{\partial v_z}{\partial t} + v_r\dfrac{\partial v_z}{\partial r} + v_z\dfrac{\partial v_z}{\partial z}\right) = -\dfrac{\partial P}{\partial z} + \eta\dfrac{1}{r}\dfrac{\partial}{\partial r}\left(r\dfrac{\partial v_z}{\partial r}\right) & \text{(10b)} \\ \dfrac{\partial P}{\partial r} = 0 & \text{(10c)} \\ \rho\left(\dfrac{\partial}{\partial t} + v_r\dfrac{\partial}{\partial r} + v_z\dfrac{\partial}{\partial z}\right)\left(c_p T + \dfrac{1}{2}v^2\right) = \dfrac{\partial P}{\partial t} + \lambda\dfrac{1}{r}\dfrac{\partial}{\partial r}\left(r\dfrac{\partial T}{\partial r}\right) & \text{(10d)} \\ P = \rho r_{He} T & \text{(10e)} \end{cases}$$

The pressure does not depend on r and given that the velocity is null at the wall (at $r = R$), the pressure gradient $\mathrm{d}P/\mathrm{d}z$ can be written as:

$$\frac{\mathrm{d}P}{\mathrm{d}z} = \eta\frac{1}{r}\frac{\partial}{\partial r}\left(r\frac{\partial v_z}{\partial r}\right)\Big|_{r=R} \tag{11}$$

The pressure variation along z-axis is then equal to the volumetric viscosity forces at the wall.

3.3. 0-D modelling of the transient rods depressurization

In order to provide boundary conditions to this 2D model of gas flow in the transient rods, a 0D model has been built. It enables to determine the mean pressure evolution in the transient rods circuit during the depressurization. This model is based on a Joule & Gay-Lussac discharge. Two tanks are separated by a valve, as presented in Fig. 5. The first tank is filled with ^{3}He. It corresponds to the gas volume located upstream the valves, mainly consisting of the transient rods. The other one is the vacuum tank downstream the valves. The section of both tanks is much higher than the flow cross section inside the valve so that the velocity inside the transient rods (~5 m/s) is negligible compared to the one in the valves (~ 10^3 m/s). We can then consider that the kinetic energy and its evolution inside the tanks are negligible.

With this assumption, we reduce the unknowns to pressure and temperature in both tanks: P_1, T_1, P_2 and T_2. The mass flowrate in the valve is expressed according to Masoneilan standards (Masoneilan, 1998):

$$Q_m = kC_v Y\left(x\right)\sqrt{xP_1\rho_1} \tag{12}$$

P_1 and ρ_1 are pressure and density at upstream conditions. k is a conversion coefficient from imperial units to international system units. $Y(x)$ is a function taking into account the compressibility of the gas when the pressure drop is increasing and C_v is the capacity of the valve. x

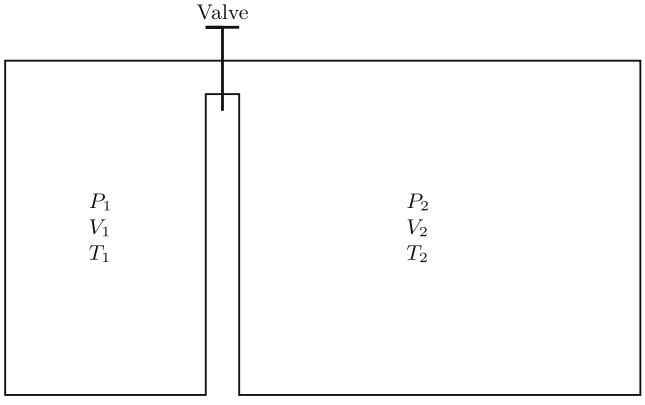

Fig. 5. Joule & Gay-Lussac discharge.

is the pressure drop ratio across the valve, equal to $\min(x_T; \Delta P/P_0)$. x_T is specific to the valve, standing for the pressure drop at which the flow becomes sonic.

The energy and mass balance in every tank leads to:

$$\begin{cases} \dfrac{\mathrm{d}\dfrac{P_1}{T_1}}{\mathrm{d}t} = -k\dfrac{C_v}{V_1}Y(x)\sqrt{xr_{He}T_1}\ \dfrac{P_1}{T_1} & (13a) \\ \dfrac{\mathrm{d}\dfrac{P_2}{T_2}}{\mathrm{d}t} = +k\dfrac{C_v}{V_2}Y(x)\sqrt{xr_{He}T_1}\ \dfrac{P_1}{T_1} & (13b) \\ \dfrac{\mathrm{d}T_1}{\mathrm{d}t} = -k\dfrac{C_v}{V_1}Y(x)\sqrt{xr_{He}T_1}\,(\gamma-1)\left(1-\dfrac{P_2}{P_1}+\dfrac{1}{2}k^2\dfrac{C_v^2}{S_c^2}Y^2(x)x\right)T_1 & (13c) \\ \dfrac{\mathrm{d}T_2}{\mathrm{d}t} = +k\dfrac{C_v}{V_2}Y(x)\sqrt{xr_{He}T_1}\,(\gamma-1)\dfrac{P_1}{P_2}\left(\dfrac{\gamma}{\gamma-1}-\dfrac{1}{\gamma-1}\dfrac{T_2}{T_1}-\dfrac{P_2}{P_1}+\dfrac{1}{2}k^2\dfrac{C_v^2}{S_c^2}Y^2(x)x\right)T_2 & (13d) \end{cases}$$

The complete demonstration of this model is accessible in Labit (2020). This model is solve with the Euler method.

The pressure evolution $P_1(t)$ is then used as the pressure boundary condition at the top of the tube.

4. Numerical solution of the analytical model

4.1. Nondimensionnalization of the equations

Before solving this system, we nondimensionnalize the equations in order to have a well scaled matrix.

The nondimensionnalized variables are:

$$\begin{cases} r^\star = \dfrac{r}{R},\quad z^\star = \dfrac{z}{L},\quad t^\star = \dfrac{t}{\tau} & (14a) \\ V_r = \dfrac{v_r}{v_0},\quad V_z = \dfrac{v_z}{v_0},\quad \Theta = \dfrac{T_w - T}{T_w - T_0},\quad \rho^\star = \dfrac{\rho}{\rho_0},\quad V^2 = V_r^2 + V_z^2 & (14b) \end{cases}$$

For the closed tube, given that the velocity is equal to 0 before the transient, the reference velocity v_0 has been taken equal to the order of magnitude of the velocity inside the rods during these transients (1 m/s). With these variables, the Eqs. (10) are nondimensionnalized:

$$\begin{cases} \Pi_1\dfrac{\partial\rho^\star}{\partial t^\star} + \dfrac{1}{r^\star}\dfrac{\partial}{\partial r^\star}(r^\star\rho^\star V_r) + \dfrac{R}{L}\dfrac{\partial}{\partial z^\star}(\rho^\star V_z) = 0 & (15a) \\ \rho^\star\left(\Pi_1\dfrac{\partial V_z}{\partial t^\star} + V_r\dfrac{\partial V_z}{\partial r^\star} + \dfrac{R}{L}V_z\dfrac{\partial V_z}{\partial z^\star}\right) - \dfrac{2}{Re_0}\dfrac{1}{r^\star}\dfrac{\partial}{\partial r^\star}\left(r^\star\dfrac{\partial V_z}{\partial r^\star}\right) = -\Pi_2\dfrac{\mathrm{d}P}{\mathrm{d}z} & (15b) \\ \rho^\star\left(\Pi_1\dfrac{\partial\Theta}{\partial t^\star} + V_r\dfrac{\partial\Theta}{\partial r^\star} + \dfrac{R}{L}V_z\dfrac{\partial\Theta}{\partial z^\star}\right) - \dfrac{2}{Pe_0}\dfrac{1}{r^\star}\dfrac{\partial}{\partial r^\star}\left(r^\star\dfrac{\partial\Theta}{\partial r^\star}\right) = \\ -\Pi_3\dfrac{\partial P}{\partial t^\star} + \Pi_4\rho^\star\dfrac{\partial\frac{1}{2}V^2}{\partial t^\star} + \Pi_5\rho^\star\left(V_r\dfrac{\partial\frac{1}{2}V^2}{\partial r^\star} + \dfrac{R}{L}\dfrac{\partial\frac{1}{2}V^2}{\partial z^\star}\right) & (15c) \\ \rho^\star = \dfrac{P}{\rho_0 r_{He}(T_w - \Theta(T_w - T_0))} & (15d) \end{cases}$$

with:

$$\begin{cases} \Pi_1 = \dfrac{R}{v_0\tau},\quad Re_0 = \dfrac{\rho_0 v_0 2R}{\eta},\quad \Pi_2 = \dfrac{R}{\rho_0 v_0^2},\quad Pe_0 = Re_0 Pr & (16a) \\ \Pi_3 = \dfrac{R}{\rho_0 v_0 \tau c_p(T_w - T_0)},\quad \Pi_4 = \dfrac{Rv_0}{c_p(T_w - T_0)\tau},\quad \Pi_5 = \dfrac{v_0^2}{c_p(T_w - T_0)} & (16b) \\ \dfrac{\mathrm{d}P}{\mathrm{d}z} = \eta\dfrac{v_0}{R^2}\dfrac{1}{r^\star}\dfrac{\partial}{\partial r^\star}\left(r^\star\dfrac{\partial V_z}{\partial r^\star}\right)\Big|_{r^\star=1} & (16c) \end{cases}$$

The pressure at every point and every time is obtained with pressure boundary condition and pressure gradient given by last equation of (16). The Nusselt number can be expressed as:

$$Nu = \frac{-2\frac{\partial\Theta}{\partial r^\star}\Big|_1}{\overline{\Theta}} \quad (17)$$

$\overline{\Theta}$ is calculated by averaging the enthalpy on the cross-section. Given that the heat capacity of a perfect gas is constant, we obtain:

$$\overline{\Theta} = \frac{1}{\int_0^1 \rho^\star V_z 2r^\star \mathrm{d}r^\star}\int_0^1 \Theta\rho^\star V_z 2r^\star \mathrm{d}r^\star \quad (18)$$

4.2. Discretization of the equations and numerical calculation scheme

Equations are discretized with finite differences method. We consider Cartesian meshes with a step $\Delta r^\star$ along r and $\Delta z^\star$ along z. The time step is $\Delta t^\star$. The radial mesh index is i, the axial mesh index is j and the time step index is n. Field A is discretized as:

$$\begin{cases} \dfrac{\partial A}{\partial t^\star} = \dfrac{A_{i,j,n} - A_{i,j,n-1}}{\Delta t^\star} & (19a) \\ \dfrac{\partial A}{\partial r^\star} = \dfrac{A_{i,j,n} - A_{i-1,j,n}}{\Delta r^\star}\ \text{For advective terms} & (19b) \\ \dfrac{\partial A}{\partial z^\star} = \dfrac{A_{i,j,n} - A_{i,j-1,n}}{\Delta z^\star}\ \text{For advective terms} & (19c) \\ \dfrac{\partial A}{\partial r^\star} = \dfrac{A_{i+1,j,n} - A_{i-1,j,n}}{2\Delta r^\star}\ \text{For diffusive terms} & (19d) \\ \dfrac{\partial^2 A}{\partial r^{\star 2}} = \dfrac{A_{i+1,j,n} - 2A_{i,j,n} + A_{i-1,j,n}}{\Delta r^{\star 2}}\ \text{For diffusive terms} & (19e) \end{cases}$$

The scheme is implicit. Advective terms (*i.e.* $\vec{v}\cdot\overrightarrow{\mathrm{grad}}A$ terms) are then discretized with a first-order upwind scheme. Diffusive terms (*i.e.* ΔA terms) are discretized with second-order centered finite difference scheme. At the wall, diffusive terms are discretized as:

$$\begin{cases} \left.\frac{\partial A}{\partial r^\star}\right|_{N_r} = \frac{A_{N_r-2,j,n} - 4A_{N_r-1,j,n}}{2\Delta r^\star} & (20a) \\ \left.\frac{\partial^2 A}{\partial r^{\star 2}}\right|_{N_r} = \frac{A_{N_r-2,j,n} - 2A_{N_r-1,j,n}}{\Delta r^{\star 2}} & (20b) \end{cases}$$

Which is still accurate to the order 2 for first derivative and to the order 1 for second derivative.

In order to solve this system, an iterative process is used. The velocity occurring in non linear terms (advection, kinetic energy) is taken equal to the velocity at the previous iteration. Every time step is calculated until residuals become lower than 10^{-6} in accordance with the Picard iterative process.

This allows to build a matrix **M** with several blocks that contain the discretization of the equation in every mesh as well as the boundary conditions. We solve with MATLAB the equation:

$$\mathbf{M}X = B \quad (21)$$

B contains the right member of the Eqs. (15) and boundary conditions. The vector X gathers the unknowns:

$$X = \begin{bmatrix} \rho^\star \\ V_r \\ V_z \\ \Theta \end{bmatrix} \quad (22)$$

5. Results of the numerical model

5.1. Open tube

5.1.1. Boundary conditions

In order to validate our model, we first study the case of a gas flowing in an open tube and compare the results to analytical velocity profile and Nusselt number. Boundary conditions for this study are presented in Fig. 6. They consist in symmetry relations at the center of the tube and Dirichlet boundary condition at the wall. Uniform velocity and temperature profiles are set at the entrance of the tube ($v_z = v_0, T = T_0$). We set $v_0 = 5$ m/s, in order to have a laminar flow with $Re = 400$. The flow is freely developing along z without outlet boundary condition. For this first validation stage, the flow is incompressible. In order to simulate an incompressible flow, the temperature difference between the wall and the fluid at the inlet is low (5 °C). The gas density (and so the pressure) is a boundary condition at the tube inlet.

5.1.2. Validation of the model

The mesh number is set to $N_r = N_z = 20$. It is derived from convergence studies that revealed that, for $N_r \geqslant 20$, results for Nusselt number, temperature and velocity converge. In order to validate this model, numerical results have to be in accordance with the literature. The Nusselt number for a thermally established flow must be equal to 3.66. Moreover, the velocity profile at the outlet must be a Poiseuille profile, and the head loss must be consistent with the Darcy–Weisbach coefficient for laminar flow ($64/Re$).

These validation elements are presented in Fig. 7. The numerical model gives a good adequation with theoretical results. The velocity profile is correct, as well as the head loss in the established flow. Concerning the heat exchanges, the Nusselt number is very close to the theoretical value of 3.656 (Nusselt, 1910) (at only 0.2%). Regarding these results, we can consider that this model is validated.

Additional results are presented in Fig. 8 and are consistent with results drawn from literature for similar conditions (Santos and Figueiredo, 2007; Presler, 1971). The radial velocity follows a consistent profile with negative values (Santos and Figueiredo, 2007). The axial velocity profile is correctly developing, as well as the temperature profile (Presler, 1971). In addition to that, we can see that the fluid is heating as it goes along the tube, what is consistent. These results give a good confidence in this numerical model.

The objective is now to model the depressurization of a single tube of the transient rods in CABRI and then to deduce a correlation for the Nusselt number in the transient rods.

5.2. Transient rods tube

5.2.1. Initial and boundary conditions

The study is slight more complex. We have to study the depressurization of ^{3}He in a tube, that is closed at the bottom and open at the top. In order to do that, we study the depressurization of a single transient rods tube of 1.5 m long and 8.8 mm in diameter. The situation is the one described in Fig. 9.

This model demands a specific boundary condition at the top of the tube. In that objective, we chained the 0D model with the 2D model.

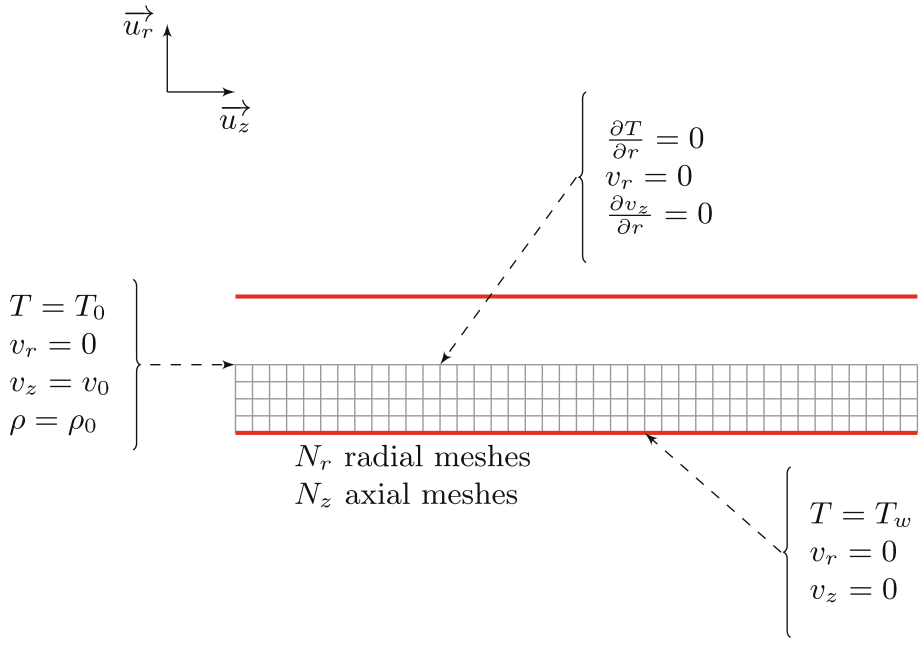

Fig. 6. Boundary conditions for an open tube.

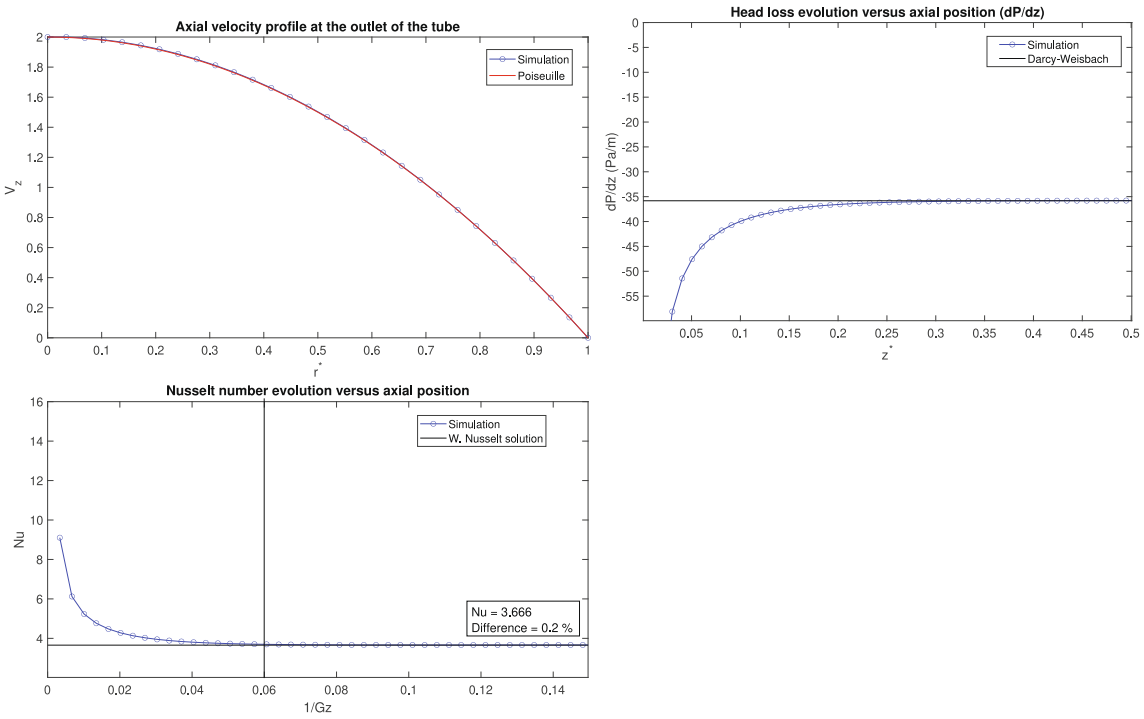

Fig. 7. Validation of the numerical model with a open tube at constant temperature.

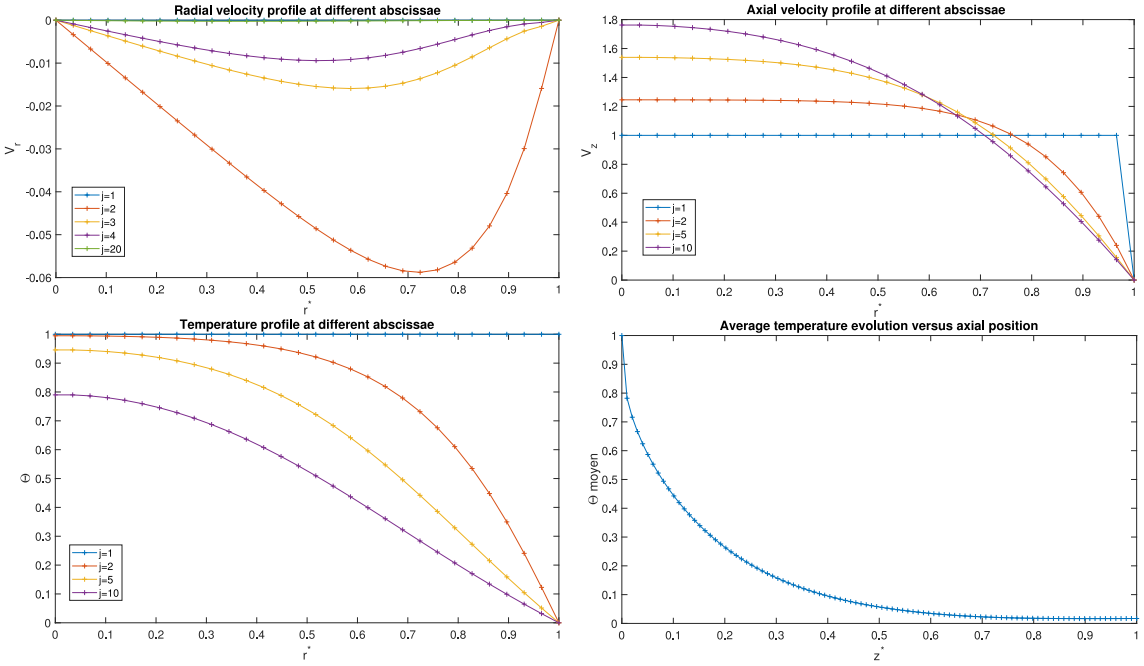

Fig. 8. Results for an open tube at constant temperature.

This is sufficient to provide a pressure boundary condition at the top of the tube.

Concerning the initial conditions, we have, everywhere in the tube:

$$\begin{cases} T = T_0 & (21a) \\ v_z = 0 & (21b) \\ v_r = 0 & (21c) \\ P = P_0 & (21d) \end{cases}$$

5.2.2. Results in a transient rods tube

The physical time step is set to 1 ms. The mesh number is set to $N_r = N_z = 20$. It has been chosen after convergence studies.

The study has been done for a SD2, with $P_0 = 5$ bar and the valve stem position (*i.e.* the aperture) $h_{04} = 2.61$ mm. Results are presented in Fig. 10. First, we can see that the total mass inside the tube decreases, as well as the temperature at the beginning of the depressurization (*i.e.* Θ increases), before increasing with the influence of the heat exchanges. The velocity slowly increases everywhere in the tube before decreasing when the gas rarefies. The last graph presents the Nusselt number at two different abscissae. The final value reached is around 5.62, larger than the usual value (3.66) used in CATHARE2. We can also observe that the

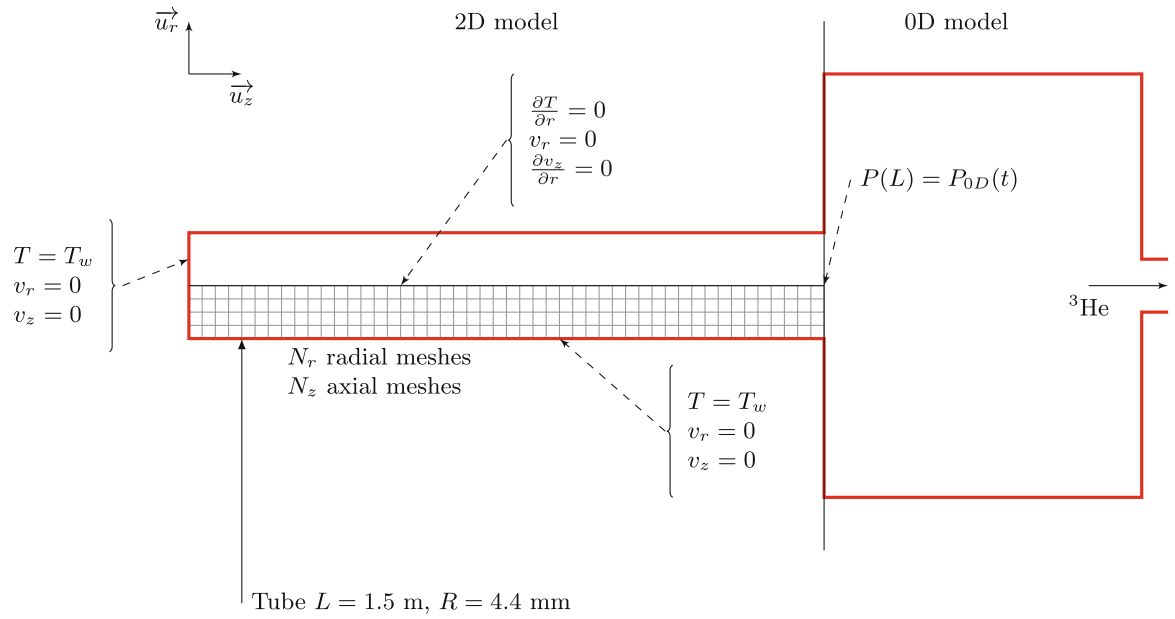

Fig. 9. Modelling of the depressurization of a single tube of the transient rods with 0D–2D models chaining.

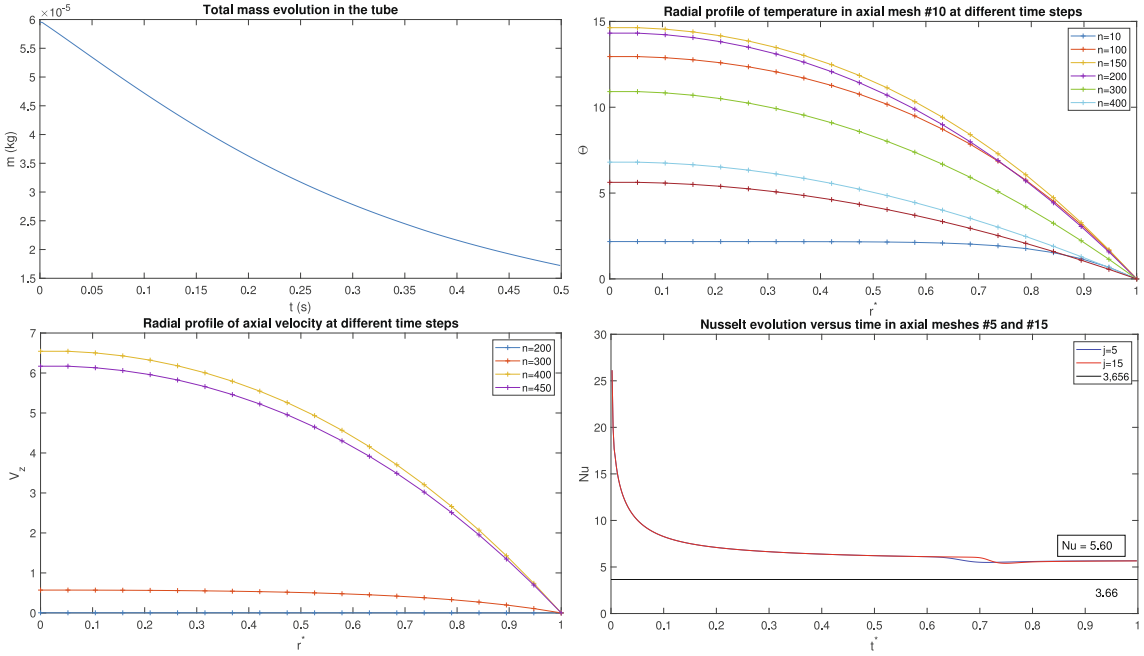

Fig. 10. Results for the depressurization of the tube.

duration of the time dependence of the Nusselt number is not necessarily negligible ($t < 0.35$ s). Furthermore, the Nusselt number does not significantly depends on the abscissa z.

These results are consistent and a rough comparison with CATHARE2 modeling helps to verify the consistency of the trend of these variables as well as other variables: mass flowrate as a function of time, pressure evolution etc. This comparison gives us a good confidence in this model and in its relevance for the depressurization modelling.

5.2.3. *Elaboration of the Nusselt number correlation*

Regarding these results, we can see that Nusselt number does not significantly depend on abscissa z inside the tube. We observe a small deviation around $t^\star = 0.7$ but very negligible in comparison with the time dependence of Nusselt number before that time. In order to reduce the number of variables, we study the time evolution of an axially-averaged Nusselt:

$$\overline{Nu}(t^\star) = \int_0^1 Nu(z^\star, t^\star)\mathrm{d}z^\star \tag{22}$$

Moreover, we have seen that the *Nu* decreases with time whereas the Reynolds number inside the tube is near zero. The singularity (at $t^\star = 0.7$ on Fig. 10) is due to a fast increase of the Reynolds number. The fast increase of *Re* is due to the evolution of the pressure gradient inside the tube. At the beginning of the transient, the pressure is identical everywhere inside the tube. There is no gradient and the pressure decreases only because the pressure at the outlet decreases (*i.e.* pressure that downstream fluid applies on fluid inside the tube), without any gas flow inside the tube, except at the outlet. When the pressure gradient

commences to increase, the gas in the tube starts to flow towards the outlet. This increases the pressure loss and then the pressure gradient, leading to *Re* fast increase. *Re* decreases when gas rarefies.

We can thus consider that, before that time, the time-dependence is due to the transient conduction in the fluid. The gas temperature decreases very fast whereas the wall temperature remains constant. The problem boils down to a transient conduction problem with a wall at a constant temperature and a fluid for which the temperature decreases very fast. The analytical resolution of this problem is difficult, but the identification of the phenomenon allows to identify the variables that could influence the heat exchanges. Hence, we tried to find a relation between Nu, Θ (temperature evolution) and *Fo* (Fourier number inside the rods, characterizing the conductive heat exchanges inside the rods):

$$\overline{Nu} = f\left(\Theta, Fo\right) \tag{23}$$

This method allows to notice that, during the depressurization and during the gas temperature decrease:

$$\frac{\overline{Nu}}{\ln\overline{\Theta}} = a\frac{1}{Fo_0} + b \tag{24}$$

Where Fo_0 is the Fourier number inside the gas at standard conditions for temperature and pressure:

$$Fo_0 = \frac{\alpha_0 t}{D_h^2} \tag{25}$$

Coefficients *a* and *b* depend on the depressurization. Given that this correlation will be used for CABRI transient rods only, these coefficients are expressed as a function of the initial pressure and the valve stem position noted h_{04}. Both parameters are experimental parameters, set before the experiment in CABRI reactor (Labit et al., 2020b). We obtain:

$$\overline{Nu} = \max\left(5.62; \left[a\frac{1}{Fo_0} + b\right]\ln\overline{\Theta}\right) \tag{26}$$

with:

$$\begin{cases} a = \left(8.6610^{-3}h_{04}^2 - 1.2010^{-3}h_{04} + 1.5910^{-2}\right)P_0^{0.3} & \text{(29a)} \\ -2.0910^{-3}h_{04}^2 + 1.3310^{-2}h_{04} - 0.38 & \\ b = -0.23h_{04}^{0.5} + 2.17 & \text{(29b)} \end{cases}$$

where P_0 is the initial pressure (in Pa) and h_{04} the valve stem position (in mm). This correlation has been established for $t > 0.01$ s for the 16 transients that have been studied (cf. Fig. 11). The results of this correlation are compared to numerical results in Fig. 11. We can see that most points embrace at ±25% the correlation. Some points are out of this domain. It is due to the fast *Re* increasing previously observed, before *Nu* reaches the value of 5.62. This is a harmless lack given that, as seen in Fig. 10 and discussed before, the deviation at this point is very low and short. The behaviour of the correlation is very good for $Nu \in [5; 15]$. The values greater than 15 correspond to the beginning of the depressurization ($t < 0.01$ s). This does not jeopardize the results.

However, it appears that the points of a single calculation are not randomly dispersed around the correlation results. Some of them are entirely above the curve, and others are under the curve. This is due to the fit of the parameters of the correlation or the form of the Eq. (26). The discrepancy is lower than 10%, but that could be improved.

6. CABRI modelling improvement

This correlation Eq. (26) has been implemented in CATHARE2. Its effect has been studied on 2 SD2 and 2 DD, whose experimental features are given in 1.

Table 1
CABRI transient experimental features.

Transient	Max Power [MW]	Energy deposit [MJ]	FWHM [ms]
SD2 7 bar 3.81 mm	1405	125	33.5
SD2 14.5 bar 5.33 mm	4785	133	20
DD 9 bar 3.81 mm	1989	167	69.5
DD 14.5 bar 3.81 mm	4884	201	30.6

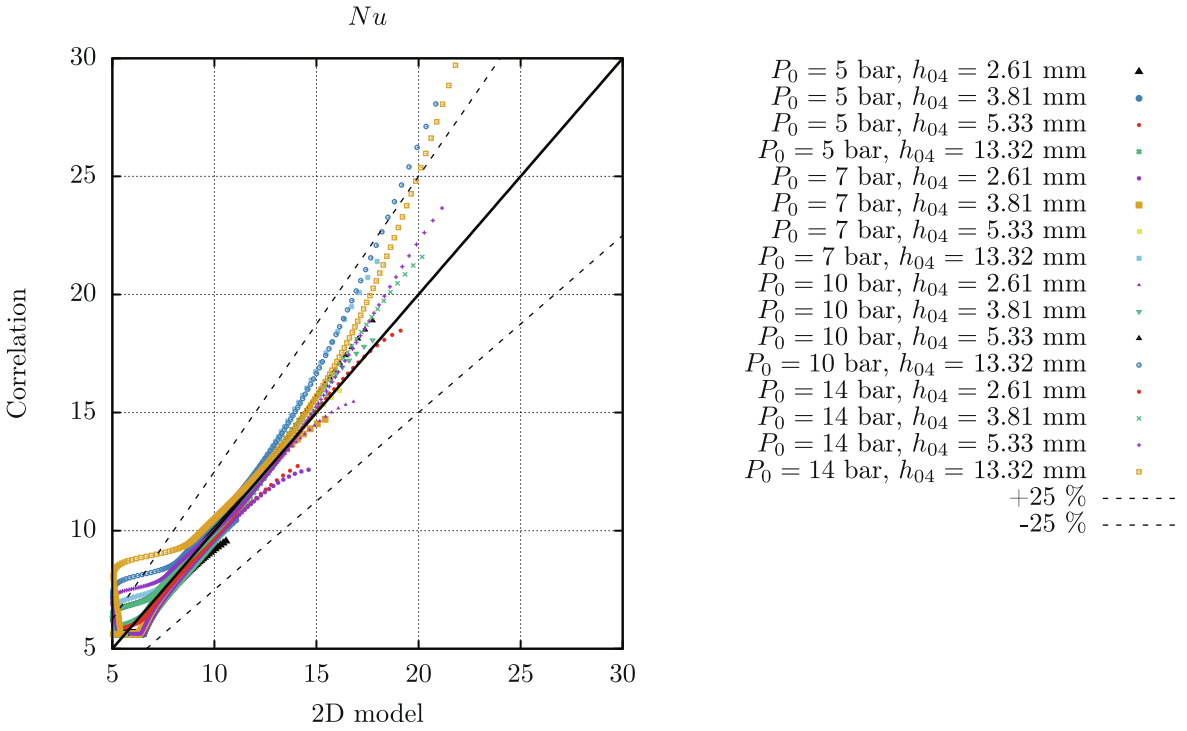

Fig. 11. Results the correlation compared to simulation results.

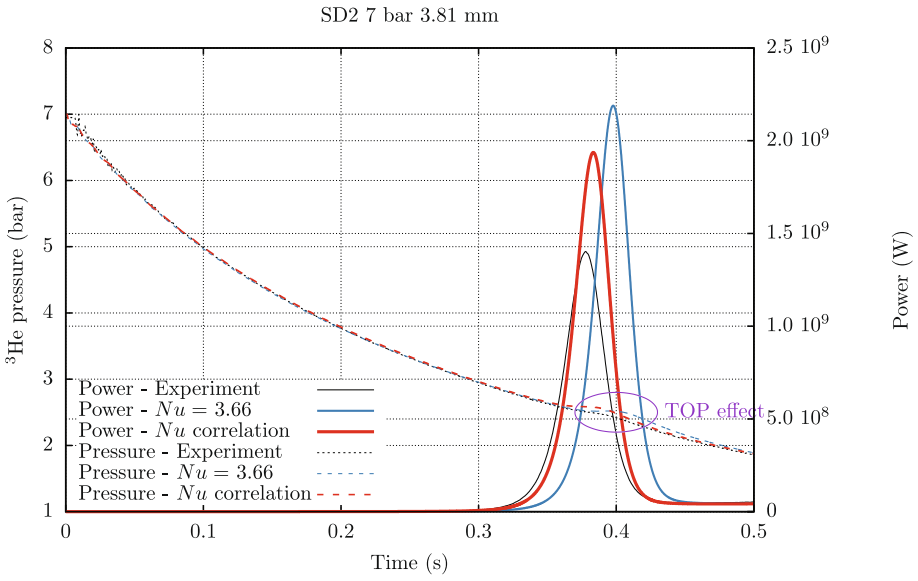

Fig. 12. Effect of the correlation on a SD2 7 bar 3.81 mm.

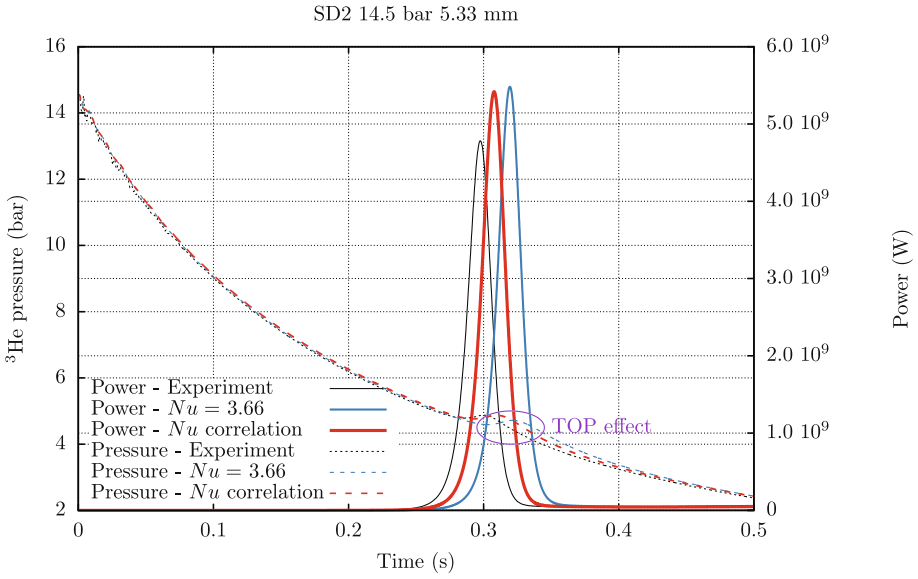

Fig. 13. Effect of the correlation on a SD2 14.5 bar 5.33 mm.

6.1. *Effect on SD2*

The effect of this correlation is noticeable on SD2. We can see in Fig. 12 and 13 that the slight delay of the power pulse that we used to observe with $Nu = 3.66$ is reduced. The TOP effect, perceptible on the pressure evolution during the pulse, is lower with the new correlation, because the gas density inside the rods is lower. The additional reactivity insertion due to TOP effect is lower. Thus the maximal power is lower and the new correlation gives a better consistency with the experiment.

6.2. *Effect on DD*

The effect is clearly considerable on the modelling of double-depressurization. With classical values of Nusselt number for laminar flows, the power pulse could be 4 times higher than the experiment, and the FWHM 2 times lower than the experiment. Figs. 14 and 15 illustrate this phenomenon. We can see in Fig. 14 that the power increase kinetics is in perfect adequation with the experiment by using the new correlation eq. (26). The shape of the power evolution (with two pulses) is reproduced, even if it is extremely sensitive to the heat exchanges. We can see in Fig. 15 that a little variation of the Nusselt number inside the rods (+ 10%) changes significantly the kinetics of the reactivity insertion.

6.3. *Discussion*

The major necessity of the improvement of the modelling of the wall/gas heat exchanges inside the transient rods is revealed throughout the modelling of SD2 and DD. These studies confirm the quality of the results obtained with the new correlation (26). Moreover, they show the high sensitivity of the results to the heat exchange coefficient. Computation/experiment differences are presented in Table 2 and compared to their value with classical value of Nusselt number for laminar flows. We can see that the new correlation helps to improve the simulation of the power pulses. Maximal power, energy deposit and FWHM (or the total width at half-maximum in the case of double pulses – DD) are in better

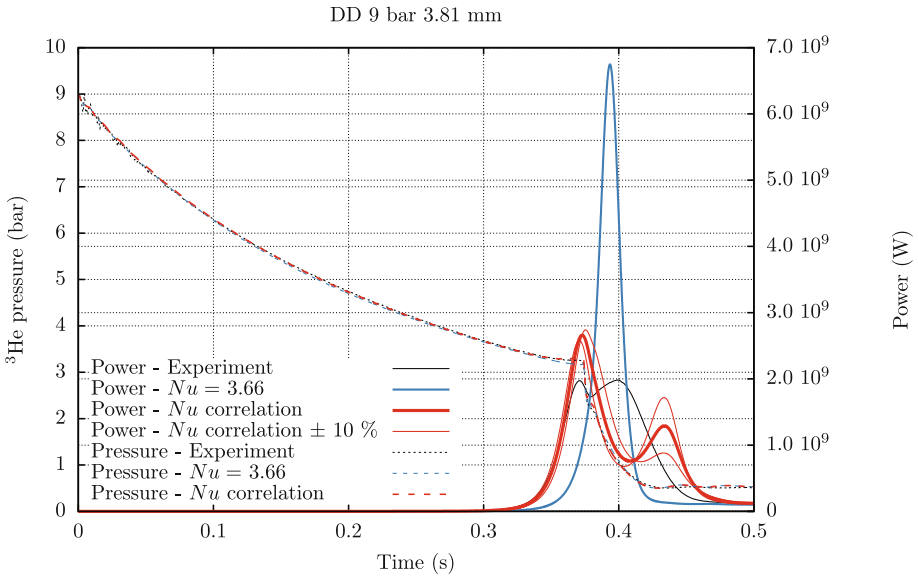

Fig. 14. Effect of the correlation on a DD 9 bar 3.81 mm.

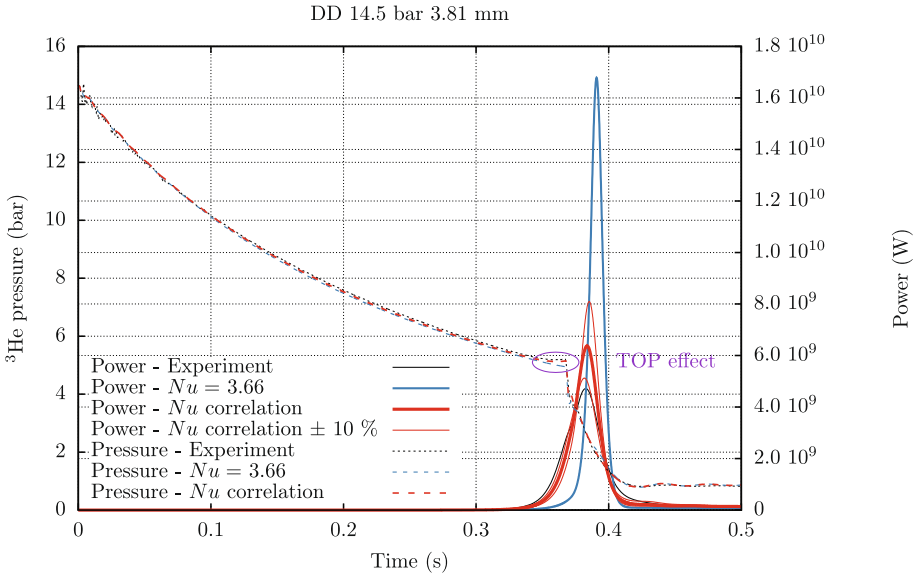

Fig. 15. Effect of the correlation on a DD 14.5 bar 3.81 mm.

Table 2
Computation/experiment differences.

Transient	Maximal difference					
	Power		Energy deposit		FWHM	
	$Nu =$ 3.66	Eq. (26)	$Nu =$ 3.66	Eq. (26)	$Nu =$ 3.66	Eq. (26)
SD2 7 bar 3.81 mm	+56%	+38%	−7%	−8%	−14%	−11%
SD2 14.5 bar 5.33 mm	+15%	+13%	+11%	+9%	−1.5%	−1.5%
DD 9 bar 3.81 mm	+226%	+34%	+1%	−4%	−74%	+12%
DD 14.5 bar 3.81 mm	+246%	+31%	+21%	−4%	−65%	−31%

agreement with the experiment. The effect is much more important for DD, where the maximal power can be reduced by a factor 8 and the energy deposit by a factor 5.

7. Conclusion and prospects

CABRI transients modelling on a multiphysic way raises many issues. Even if the CATHARE2 tool has been modified in order to better manage neutronic (Labit et al., 2020b), transient thermalhydraulic (Labit et al., 2020a) and thermomechanic phenomena, the modelling of "slow" depressurizations like SD2 and more particularly double-depressurizations was still not accurate enough. Physical analyses and studies have shown that the effect of the heat exchanges inside the transient rods were very important for the reproductibility of the power pulse during these transients, where the flow remains laminar inside the tubes of the transient rods. As a consequence, laminar heat exchanges have been studied on a theoretical point of view and, after some literature reviews, the choice has been made to build an analytical model of the depressurization of ^{3}He in these tubes. A 3D (2-D axissymetric) analytical model has been developed in order to obtain the value of the Nusselt number inside the transient rods during the depressurization.

This model has been numerically (by finite-difference method)

solved with MATLAB. After a first step, whose the aim was the validation of this tool, the resolution of the equations describing the flow during the depressurization revealed that the Nusselt number inside the rods is highly dependent on time, but not really on axial position. This has led us to conclude that this effect was due to transient conduction inside the gas of the transient rods tube. As previously observed for the heat exchanges inside the core (Labit et al., 2020b), usual steady-state correlations reach their limits during CABRI transients.

A newly established correlation has then been developed in order to be implemented in CATHARE2. It has been tested and new results are very satisfactory. The experiment/simulation difference on maximal power is reduced by a factor up to 10. New simulations are then in better adequation with the experiment (around 30% on maximal power). Nevertheless, results are highly sensitive to heat exchanges inside the rods, and given that phenomena are strongly coupled during these transients, the improvement of the multiphysic modelling of CABRI transients is necessary. For instance, the helium density evolution during SD2 and DD is relatively slow. That leads to neutron flux distribution and spectrum evolutions that can have significant effects and that can influence neutronic feedbacks, and then the power evolution. That point will be diligently investigated in a near future.

Declaration of Competing Interest

The authors declare that they have no known competing financial interests or personal relationships that could have appeared to influence the work reported in this paper.

Acknowledgements

This work has been achieved in the framework of the CEA-EDF-Framatome-IRSN partnership. The authors would like to particularly thank IRSN which leads the CABRI International Program.

References

Labit, J.-M., Marie, N., Merle, E., Clamens, O., 2020a. Transient heat exchanges under fast Reactivity-Initiated Accident. Nucl. Eng. Design, 110917. https://doi.org/10.1016/j.nucengdes.2020.110917.

Labit, J.-M., Marie, N., Merle, E., Clamens, O., 2020b. Multiphysics CATHARE2 modeling and experimental validation methodology against CABRI transients. Nucl. Eng. Design, 110836. https://doi.org/10.1016/j.nucengdes.2020.110836.

Hudelot, J.-P., Fontanay, E., Molin, C., Moreau, A., Pantera, L., Lecerf, J., Garnier, Y., Duc, B., 2016. CABRI facility: upgrade, refurbishment, recommissioning and experimental capacities. In: Proc. Int. Conf. PHYSOR2016, Sun Valley, USA.

Geffraye, G., Antoni, O., Farvacque, M., Kadri, D., Lavialle, G., Rameau, B., Ruby, A., 2011. CATHARE 2 V2.5_2: a single version for various applications. Nucl. Eng. Design 241 (11), 4456–4463.

Emonot, P., et al., 2011. A new system code for thermal-hydraulics in the context of the NEPTUNE project. Nucl. Eng. Design 241 (11), 4476–4481.

Labit, J.-M., Marie, N., Hudelot, J.-P., Merle, E., 2019. An advanced experimental validation methodology of multiphysics calculation tools on CABRI transients. In: Proceedings of M&C 2019, vol. 1, Portland, Oregon, pp. 2684–2695.

RELAP5/MOD3.2 code manual. Technical Report Report NUREG/CR-5535, US Nuclear Regulatory Commission, Washington DC, USA, 1995.

Austregesilo, H., Others, 2003. ATHLET models and methods. Technical Report Report GRS-P-1/Vol. 4, Gesellshaft fur Anlagen und Reaktorsicherheit, Garching, Germany.

Staudenmeier, J., 2004. TRACE: TRACE/RELAP advanced computational engine 2004. In: Transactions of the 2004 Nuclear Safety Research Conference, Number NUREG/CP-0188, pp. 25–27.

Clamens, O., 2018. Analyse et propagation des incertitudes associées à la dépressurisation de l'Hélium 3 sur les transitoires de puissance du réacteur CABRI. PhD thesis, CEA – Université Grenoble-Alpes.

Incropera, J.P., Dewitt, D.P. Fundamentals of Heat and Mass Transfer, fifth ed., Wiley.

Lamarsh, John R., 1966. Introduction to Nuclear Reactor Theory. Addison Wesley Publishing Company.

Shah, R.K., London, A.L., 1978. Laminar Flow Forced Convection in Ducts: A Source Book for Compact Heat Exchanger Analytical Data. Academic Press.

Nusselt, W., 1910. Die abhängigkeit der wärmeübergangszahl von der rohrlänge (de la dépendance du coefficient d'échange thermique á la longueur d'un tube chauffant). VDI 54, 1154–1158.

Belhocine, A., Wan Omar, W.Z., 2018. Exact solution of boundary value problem describing the convective heat transfer in fully-developed laminar flow through a circular conduit. Songklanakarin J. Sci. Technol. 40, 840–853.

Presler, A.F., 1971. Analytical and experimental study of compressible laminar-flow heat transfer and pressure drop of a gas in a uniformly heated tube. NASA TECHNICAL NOTE TN D-6333, NASA, Lewis Research Center, Cleveland, Ohio.

Masoneilan, 1998. Masoneilan Control Valve Sizing Handbook, volume Bulletin OZ1000.

Labit, J.-M., 2020. Modélisation multiphysique des transitoires d'insertion de réactivité et méthodologie de validation appliquée au réacteur CABRI. PhD thesis, CEA - Université Grenoble-Alpes.

Santos, R.G., Figueiredo, J.R., 2007. Laminar elliptic flow in the entrance region of tubes. J. Braz. Soc. Mech. Sci. Eng. 29, 233–239.